

Two-dimensional paradigm for symmetry breaking: The nonlinear Schrödinger equation with a four-well potential

C. Wang,¹ G. Theocharis,¹ P. G. Kevrekidis,¹ N. Whitaker,¹ K. J. H. Law,¹ D. J. Frantzeskakis,² and B. A. Malomed³

¹*Department of Mathematics and Statistics, University of Massachusetts, Amherst, Massachusetts 01003-4515, USA*

²*Department of Physics, University of Athens, Panepistimiopolis, Zografos, Athens 15784, Greece*

³*Department of Physical Electronics, Faculty of Engineering, Tel Aviv University, Tel Aviv 69978, Israel*

(Received 2 April 2009; revised manuscript received 27 August 2009; published 30 October 2009)

We study the existence and stability of localized modes in the two-dimensional (2D) nonlinear Schrödinger/Gross-Pitaevskii (NLS/GP) equation with a symmetric four-well potential. Using the corresponding four-mode approximation, we trace the parametric evolution of the trapped stationary modes, starting from the linear limit, and thus derive a complete bifurcation diagram for families of the stationary modes. This provides the picture of spontaneous symmetry breaking in the fundamental 2D setting. In a broad parameter region, the predictions based on the four-mode decomposition are found to be in good agreement with full numerical solutions of the NLS/GP equation. Stability properties of the stationary states coincide with those suggested by the corresponding discrete model in the large-amplitude limit. The dynamics of unstable modes is explored by means of direct simulations. Finally, in addition to the full analysis for the case of the self-attractive nonlinearity, the bifurcation diagram for the case of self-repulsion is briefly considered too.

DOI: [10.1103/PhysRevE.80.046611](https://doi.org/10.1103/PhysRevE.80.046611)

PACS number(s): 05.45.Yv, 03.75.Lm, 42.65.Tg

I. INTRODUCTION

In the recent years, experimental and theoretical studies of atomic Bose-Einstein condensates (BECs) have drawn a great deal of interest [1,2]. Many of these studies have been dealing with macroscopic nonlinear structures that arise in BECs, and often have counterparts in nonlinear optics [3]. One of the appealing features of this research area is the possibility to tailor desired geometric settings by designing appropriate magnetic, optical, or combined traps that confine the ultracold bosonic atoms. For this reason, the analysis of the structure, stability and dynamical properties of nonlinear matter-waves trapped in such geometries have become one of central topics of the studies. The theoretical analysis is enabled by the fact that a very accurate description of dilute atomic BECs is furnished, in the mean-field approximation, by the Gross-Pitaevskii (GP) equation, which is a variant of the nonlinear Schrödinger (NLS) equation. The cubic nonlinearity in the GP equation originates from collisions between atoms, which should be taken into account despite the rarefaction of the condensate. The NLS equation in this, as well as in different but related forms, is also relevant to a variety of applications in nonlinear optics and other areas [3–5].

Among the trapping configurations available to current BEC experiments, one that allows direct observation of fundamental manifestations of the intrinsic nonlinearity is the double-well potential (DWP). Its prototypical realization is provided by a parabolic (harmonic) trap combined with a periodic potential, which can be created, as an “optical lattice” (OL), by the interference of laser beams illuminating the condensate [1,2,4]. The DWP was realized experimentally in [6], using an optical dipole trap to induce the harmonic trap. The experiments reported in Ref. [6] had revealed a variety of important effects, including tunneling and Josephson oscillations in the case of a small number of atoms, as well as the macroscopic quantum self-trapping leading to a stable asymmetric partition of atoms between the

wells for a sufficiently large number of atoms, which is a manifestation of the *spontaneous symmetry breaking* (SSB) induced by the nonlinearity. Subsequent works have used the double-well setting for further fundamental studies, including, in particular, the dynamics and interactions of dark solitons [7,8]. DWPs have also inspired theoretical studies of various problems, such as finite-mode reductions, exact analytical results for specially designed shapes of the potential, quantum effects [9–17], and a *nonlinear* DWP (alias a double-well *pseudopotential*), which is induced by the spatial modulation of the nonlinearity coefficient, rather than the use of the linear potential [18]. It is relevant to mention that DWPs have also been studied in the context of nonlinear optics, including twin-core self-guided laser beams in Kerr media [19] and optically induced dual-core wave guiding structures in photorefractive crystals [20].

The aim of the present work is to extend the analysis of the DWP, and SSB effects in such settings, to a two-dimensional (2D) geometry. Unlike previous studies of the trapping of quasi-2D BECs under the combined action of harmonic traps and optical-lattice potentials [21], we consider a symmetric set of four wells, which is the most natural configuration that allows the study of the SSB in situations where the genuine 2D nature of the system plays a critical role. It is also the natural 2D extension of the above-mentioned two-well settings, considered earlier extensively, both in the theory [9–18,20] and experiment [6]. The 2D four-well BEC-trapping configuration can be created as the combination of an isotropic parabolic magnetic trap, or a similar optical dipole trap, and a cosinusoidal two-dimensional OL in BECs, in a wide range of parameters (the trapping frequency and lattice strength). The same model can be realized in optics too, using a bulk nonlinear medium with a symmetric set of four embedded waveguiding channels. Among various localized states that may be predicted in this model, those featuring the SSB are of main interest, featuring the physical manifestations of the nonlinearity in the previ-

ously unexplored 2D setting. Previously, SSB effects in the 2D geometry were studied for fundamental solitons and localized vortices in a different model, based on a set of two parallel-coupled nonlinear cores carrying full two-dimensional [22] or quasi-one-dimensional OLs (in the latter case, the lattices in the two layers may be mutually parallel [23] or perpendicular [24]). The results reported in the present paper are completely different, due to the difference in the structure of the linear couplings between the four potential wells, which form a square set, on the one hand, and between parallel 2D infinite layers, on the other.

As suggested by the aforementioned works that analyzed the SSB and related effects in the one-dimensional (1D) geometry, a natural approach to the analysis of the four-well configuration may be based on a Galerkin-type few-mode truncation that reduces the 2D GP equation to a discrete system, cf. Ref. [25]. In the framework of this approach, we generate a bifurcation diagram, with the aim to predict a global set of possible stationary states of the underlying four-well system. Then, by way of a numerical solution of the underlying GP equation, we verify that all the states predicted by the four-site reduction indeed exist in the underlying continuum model. Furthermore, in the limit of strong nonlinearity, the stability of the predicted modes coincides with what is expected from the discrete model.

The paper is structured as follows. In Sec. II, we present the model and the derivation of the four-mode approximation. Numerical results are reported in Sec. III. We report complete bifurcation diagrams of possible stationary states for both the underlying GP equation and for its four-mode reduction. Comparison between them demonstrates very good agreement, which provides for the justification of the Galerkin approximation. In addition to the study of the existence and stability, evolution of unstable modes is explored too, by means of direct numerical simulations. Finally, we summarize the findings in Sec. IV, where we also discuss possible directions for further work.

II. MODEL AND THE GALERKIN APPROXIMATION

We start by presenting the basic model in the quasi-2D setting, namely, the NLS/GP equation in (2+1)-dimensions, which can be written in the following dimensionless form [1,2,4]:

$$i\partial_t u = \hat{L}u + s|u|^2 u - \mu u. \quad (1)$$

If Eq. (1) is realized as the GP equation for a ‘‘pancake’’-shaped, i.e., effectively two-dimensional, BEC (see Ref. [26] and references therein), $u(x,y,t)$ is the normalized mean-field wave function of the condensate, μ the chemical potential, $s=+1$ and -1 correspond, respectively, to repulsive or attractive interatomic interactions, and \hat{L} is the usual single-particle operator,

$$\hat{L} = -(1/2)\Delta + V(x,y), \quad (2)$$

with the 2D Laplacian, $\Delta \equiv \partial_x^2 + \partial_y^2$, and potential $V(x,y)$. In this work, we focus on the SSB and related effects in the 2D space, for which the most natural setting, where the genuine

2D nature of the system plays a critical role, is provided by the four-well potential, that may be taken in the following form:

$$V(x,y) = \frac{1}{2}\Omega^2 r^2 + V_0[\cos(2kx) + \cos(2ky)], \quad (3)$$

with $r^2 \equiv x^2 + y^2$. This potential directly corresponds to a common experimental situation, being composed of the harmonic trap of strength Ω and OL with strength V_0 and period $d = \pi/k$. Below, we present systematic results for the following values of the parameters of the potential:

$$\Omega = 0.21, \quad V_0 = 0.5, \quad k = 0.3, \quad (4)$$

which adequately represent the generic situation. Then, the four lowest eigenvalues of operator \hat{L} with coefficients [Eq. (4)] are found to be

$$\omega_0 = 0.3585, \quad \omega_1 = \omega_2 = 0.3658, \quad \omega_3 = 0.3731. \quad (5)$$

Another physical realization of the model is possible in nonlinear optics. If t is interpreted as propagation distance, and $-\mu$ as the respective propagation constant, Eq. (1) governs the transmission of (2+1)-dimensional beams in the bulk medium with transverse coordinates (x,y) , with potential [Eq. (3)] accounting for a transverse waveguiding structure induced via local modulation of the refractive index. In optics, the self-focusing ($s=-1$) corresponds to ordinary Kerr nonlinearity; the self-defocusing nonlinearity may be possible too—in particular, in semiconductor waveguides [27], although in those cases it is accompanied by nonlinear loss.

The four-mode approximation, based on the multimode expansion of $u(x,y,t)$ and Galerkin-type truncation of higher-order modes, is relevant in the present setting provided that the wave function in the case of the BEC, or the beam in the optical waveguide, is sufficiently well trapped in the four-well potential. In the case of the self-focusing nonlinearity, $s=-1$, it is also necessary to impose a restriction on the normalized number of atoms (alias the total power of the optical beam); this quantity is defined by the norm of the wave function, namely,

$$N = \iint |u(x,y,t)|^2 dx dy, \quad (6)$$

and the restriction is: $N < N_{\text{cr}} \approx 5.84$, so as to prevent the collapse which is possible if N exceeds the critical value N_{cr} [28] (the actual bifurcation diagrams for the case we study, displayed in Fig. 3, indeed meet this condition).

We denote the ground and first three excited eigenstates of the linear operator \hat{L} , which are shown in Fig. 1, as u_0 and $u_{1,2,3}$. This set constitutes a natural minimum basis for the Galerkin truncation in the set of four potential wells coupled by tunneling. Eigenstates $u_j (j=0,1,2,3)$ can be chosen to be real, given the Hermitian nature of the operator \hat{L} . Then, solutions to Eq. (1) for values of the chemical potential taken in a vicinity of linear eigenvalues (5) may be approximated by linear combinations of the four eigenfunctions.

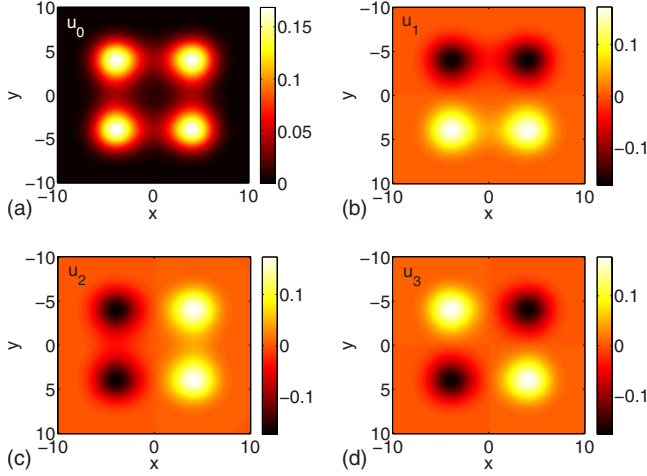


FIG. 1. (Color online) The wave functions of the ground state, u_0 , and the first three excited states, u_1 , u_2 , and u_3 , for the four-well potential of Eq. (3) with $\Omega=0.21$, $V_0=0.5$, and $k=0.3$. Note the difference in the gray-scale (color, in the online version) bars in the first and three others panels, related to the fact that the wave function of the ground state is positive, while the excited states feature sign-changing patterns.

Actually, it is more convenient to use a linearly transformed orthonormal basis, $\{\Phi_0, \Phi_1, \Phi_2, \Phi_3\}$, which is built of combined modes localized in different wells (see Fig. 2),

$$[\Phi_0 \ \Phi_1 \ \Phi_2 \ \Phi_3] = [u_0 \ u_1 \ u_2 \ u_3]T, \quad (7)$$

where the transformation matrix is

$$T = \frac{1}{2} \begin{pmatrix} 1 & 1 & 1 & 1 \\ -1 & -1 & 1 & 1 \\ -1 & 1 & 1 & -1 \\ 1 & -1 & 1 & -1 \end{pmatrix}. \quad (8)$$

Using the new basis, we define the four-mode decomposition as

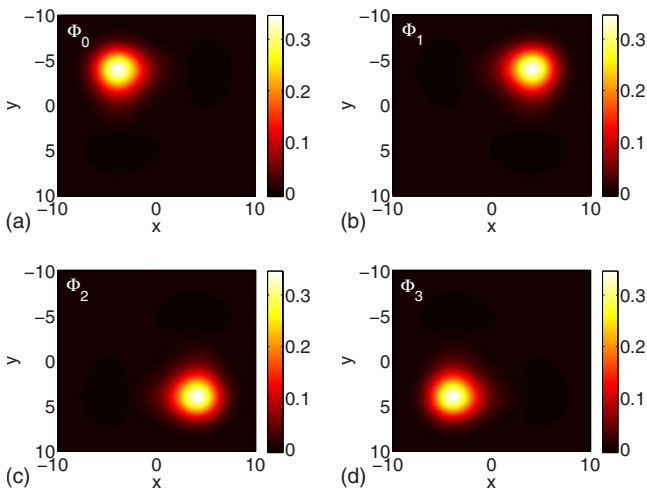


FIG. 2. (Color online) Basis modes $\{\Phi_0, \Phi_1, \Phi_2, \Phi_3\}$ that are localized in each of the wells.

$$u(x, y, t) = \sum_{j=0}^3 c_j(t) \Phi_j(x, y), \quad (9)$$

with time-dependent complex amplitudes $c_j(t)$, $j=0, 1, 2, 3$. Substituting Eq. (9) into Eq. (1) and projecting onto basis $\{\Phi_0, \Phi_1, \Phi_2, \Phi_3\}$, we derive, by means of straightforward algebra, the following system of four ordinary differential equations (ODEs),

$$\begin{aligned} i\dot{c}_j = & \tilde{\omega}_j + sA_j|c_j|^2c_j + s \sum_{k \neq j} B_{jk}(2|c_k|^2c_j + c_k^2c_j^*) \\ & + s \sum_{k \neq j} [D_{jk}|c_k|^2c_k + D_{jk}(2|c_j|^2c_k + c_j^2c_k^*)] \\ & + s \sum_{k \neq l \neq j \neq k} E_{kjl}(2|c_k|^2c_l + c_k^2c_l^*) + sG \sum_{k \neq l \neq j \neq k} E_{jkl}(c_j^*c_kc_l \\ & + c_jc_k^*c_l + c_jc_kc_l^*) + s \sum_{\substack{k \neq l \neq m \neq k \\ k, l, m \neq j}} c_k^*c_l c_m, \end{aligned} \quad (10)$$

with the summation performed over $k, l, m=0, 1, 2, 3$. To cast these equations in a more compact form, we have defined

$$\begin{bmatrix} \tilde{\omega}_0 \\ \tilde{\omega}_1 \\ \tilde{\omega}_2 \\ \tilde{\omega}_3 \end{bmatrix} = \frac{1}{4} \begin{bmatrix} \gamma_0 - 4\mu & \gamma_1 & \gamma_3 & \gamma_2 \\ \gamma_1 & \gamma_0 - 4\mu & \gamma_2 & \gamma_3 \\ \gamma_3 & \gamma_2 & \gamma_0 - 4\mu & \gamma_1 \\ \gamma_2 & \gamma_3 & \gamma_1 & \gamma_0 - 4\mu \end{bmatrix} \begin{bmatrix} c_0 \\ c_1 \\ c_2 \\ c_3 \end{bmatrix}, \quad (11)$$

where $\gamma_0 \equiv \omega_0 + \omega_1 + \omega_2 + \omega_3$, $\gamma_1 \equiv \omega_0 + \omega_1 - \omega_2 - \omega_3$, $\gamma_2 \equiv \omega_0 - \omega_1 + \omega_2 - \omega_3$, and $\gamma_3 \equiv \omega_0 - \omega_1 - \omega_2 + \omega_3$. Notice that, for the particular eigenvalues (5), one has $\gamma_1 = \gamma_2 = \omega_0 - \omega_3$ and $\gamma_3 \approx 0$. The nonlinear coefficients in Eq. (10) are given by overlap integrals, viz., $A_n \equiv \iint \Phi_n^4 dx dy$, $B_{mn} \equiv \iint \Phi_m^2 \Phi_n^2 dx dy$, $D_{mn} \equiv \iint \Phi_m^3 \Phi_n dx dy$, $E_{lmn} \equiv \iint \Phi_l^2 \Phi_m \Phi_n dx dy$, $G \equiv \iint \Phi_0 \Phi_1 \Phi_2 \Phi_3 dx dy$, with $l, m, n=0, 1, 2, 3$; these indices must be mutually different wherever they appear in the coefficients attached to the nonlinear terms.

For our choice of the parameters of the potential, the overlapping between modes Φ_i is weak (see Fig. 2), therefore all other overlap integrals are much smaller than the A_n 's. For example, $A_n = 0.0585$, $n=0, 1, 2, 3$, $B_{01} = 4.72 \times 10^{-5}$, $B_{02} = 3.82 \times 10^{-8}$, $D_{01} = -5.5 \times 10^{-4}$, $D_{02} = 5.17 \times 10^{-6}$, $E_{012} = -4.44 \times 10^{-7}$, $E_{013} = 5.17 \times 10^{-6}$, and $G = 3.82 \times 10^{-8}$. Other overlap integrals are similar to the ones listed above due to the symmetry of the Φ_i 's. Neglecting these small overlap terms leads to the following simplification of Eq. (10),

$$i\dot{c}_j = \tilde{\omega}_j + A_j|c_j|^2c_j, \quad j=0, 1, 2, 3, \quad (12)$$

in which the $\tilde{\omega}_j$'s are linear combinations of the c_j 's as explained in Eq. (11). It has been checked that this simplification of the four-mode equations very slightly affects the accuracy of the solutions, while it renders the identification of various bifurcation branches significantly easier. Furthermore, this reduction is more useful, as we may use respective solutions as inputs for generating numerical solutions of the full GP system, as explained below. In general terms, what can be said about the validity of the four-mode approxima-

tion is the following: as long as the chemical potential μ remains close to the first few eigenvalues ω_0 - ω_3 of the linear limit (i.e., low nonlinearity), we expect the approximation to be quite accurate. Furthermore, the wider the distance of these eigenvalues from subsequent linear spectrum eigenvalues (upon suitable selection of the barrier height and interwell distance), again the more accurate this approximation is expected to be.

In this 2D setting, we seek for real and complex stationary solutions to the ODE system. Substituting $c_j(t) \equiv \rho_j(t)e^{i\varphi_j(t)}$ into Eq. (12), we split them into real equations for ρ_j and φ_j ,

$$\dot{\rho}_0 = \frac{1}{4} \gamma_1 [\rho_1 \sin(\varphi_1 - \varphi_0) + \rho_3 \sin(\varphi_3 - \varphi_0)], \quad (13)$$

$$\dot{\varphi}_0 = \left(\mu - \frac{1}{4} \gamma_0 \right) - s A_0 \rho_0^2 - \frac{1}{4} \gamma_1 \times \left[\frac{\rho_1}{\rho_0} \cos(\varphi_1 - \varphi_0) + \frac{\rho_3}{\rho_0} \cos(\varphi_3 - \varphi_0) \right], \quad (14)$$

$$\dot{\rho}_1 = \frac{1}{4} \gamma_1 [\rho_0 \sin(\varphi_0 - \varphi_1) + \rho_2 \sin(\varphi_2 - \varphi_1)], \quad (15)$$

$$\dot{\varphi}_1 = \left(\mu - \frac{1}{4} \gamma_0 \right) - s A_1 \rho_1^2 - \frac{1}{4} \gamma_1 \times \left[\frac{\rho_0}{\rho_1} \cos(\varphi_0 - \varphi_1) + \frac{\rho_2}{\rho_1} \cos(\varphi_2 - \varphi_1) \right], \quad (16)$$

with the equations for $\rho_{2,3}$ and $\varphi_{2,3}$ obtained by interchanging the indices, $0 \leftrightarrow 2$ and $1 \leftrightarrow 3$, except for γ_0 and γ_1 .

Looking for stationary solutions with constant amplitudes ρ_j , and phases φ_j which are integer multiples of π , we reduce Eqs. (13)–(16) to a set of four algebraic equations for ρ_j , which can be used to derive a complete set of stationary modes of the four-mode truncation. These were further used as initial guesses to generate numerical solutions of the full system of the GP equations. Moreover, our analysis of the four-mode system indicates that nontrivial complex solutions in this setting are possible in the form of *discrete vortices*, i.e., solutions with phase sets $\varphi_j = \pi j/2$, $j=0,1,2,3$ [29], which have been studied in detail in Refs. [21,30] (we also briefly consider them here).

III. NUMERICAL RESULTS

A. Attractive interactions

We begin the presentation of results obtained from the analysis of both Eq. (1) and the four-mode truncation, Eqs. (13)–(16) for the case of the self-focusing nonlinearity, i.e., $s=-1$. To solve Eq. (1) numerically, we applied Newton's fixed point iteration method with tolerance 10^{-8} . The basic bifurcation diagram, presented in Fig. 3, displays the norm [Eq. (6)] as a function of the chemical potential, μ (or the total power versus the propagation constant, in terms of the optical waveguide). The top left panel of Fig. 3 presents the full numerically found diagram, which involves twelve real

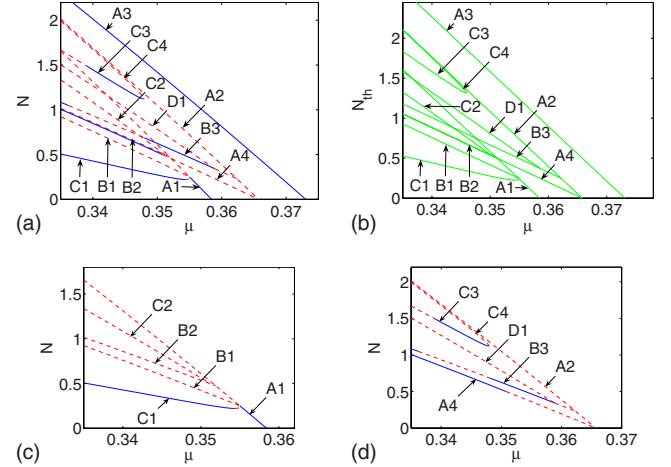


FIG. 3. (Color online) Top panels: norm N of numerically found solutions of Eq. (1) (left), and their counterparts predicted by the four-mode approximation (right), for the attractive nonlinearity ($s=-1$), as a function of chemical potential μ . The bottom panels are segments of the top left panel, given in order to clarify the details of the relevant bifurcation picture. The (blue) solid curves and (red) dashed curves denote stable and unstable solutions, respectively. The meaning of branches is explained in the text, their profiles and stability being detailed in Figs. 4–7.

and one complex solution branches (for the latter one, N is the same as for one of the real branches, hence this branch is not visible as a separate curve in the diagram). The companion diagram in the top right panel is obtained from the stationary version of Eqs. (13)–(16), demonstrating good agreement with its numerical counterpart. Although the relevant diagram contains (solely) the existence information regarding the corresponding branches of solutions, we have checked that the stability features of the four-mode picture are in line with those of the full NLS/GP model, wherever appropriate. The only feature that is missed by the four-mode description (below) that cannot be tracked within this reduced framework.

The 12 real branches are labeled, mainly, according to their relation to the respective populations of the four wells (i.e., the distribution of the total norm between the wells). To fix the notation, we introduce a symbolic representation in the form of 2×2 matrices, labeling different types of the waveforms that arise in the diagram, as follows: $A1 \equiv \begin{pmatrix} 1 & 1 \\ 1 & 1 \end{pmatrix}$, $A2 \equiv \begin{pmatrix} 1 & 1 \\ -1 & -1 \end{pmatrix}$, $A3 \equiv \begin{pmatrix} -1 & 1 \\ 1 & -1 \end{pmatrix}$, $A4 \equiv \begin{pmatrix} 1 & 0 \\ 0 & -1 \end{pmatrix}$, $B1 \equiv \begin{pmatrix} 1 & 1 \\ \varepsilon & \varepsilon \end{pmatrix}$, $B2 \equiv \begin{pmatrix} 1 & \varepsilon \\ \varepsilon & 1 \end{pmatrix}$, $B3 \equiv \begin{pmatrix} 1 & -1 \\ \varepsilon & -\varepsilon \end{pmatrix}$, $C1 \equiv \begin{pmatrix} 1 & \varepsilon \\ \varepsilon & \varepsilon \end{pmatrix}$, $C2 \equiv \begin{pmatrix} 1 & \varepsilon \\ 1-\varepsilon & 1 \end{pmatrix}$, $C3 \equiv \begin{pmatrix} 1 & -\varepsilon \\ -1-\varepsilon & 1 \end{pmatrix}$, $C4 \equiv \begin{pmatrix} 1-\varepsilon & 1 \\ 1 & -1-\varepsilon \end{pmatrix}$, and $D1 \equiv \begin{pmatrix} 1 & 1-\varepsilon \\ -1-\varepsilon & -\varepsilon \end{pmatrix}$. In this representation, the symbol 0 means that the particular well is not populated, while +1 and -1 indicate it is populated with the phase of the wave function equal to 0 or π respectively. The symbol ε , where $0 < \varepsilon \ll 1$, (i.e., ε is a nonvanishing quantity much smaller than 1), denotes a small (but nonzero) population in one of the wells. This symbol is also used to denote the SSB effect, when the density peaks feature values $\pm 1 \pm \varepsilon$, which are slightly different from those corresponding to ± 1 . The labeling is then defined as follows: branches A1-A4 have equal amplitudes in all the wells which are designated as

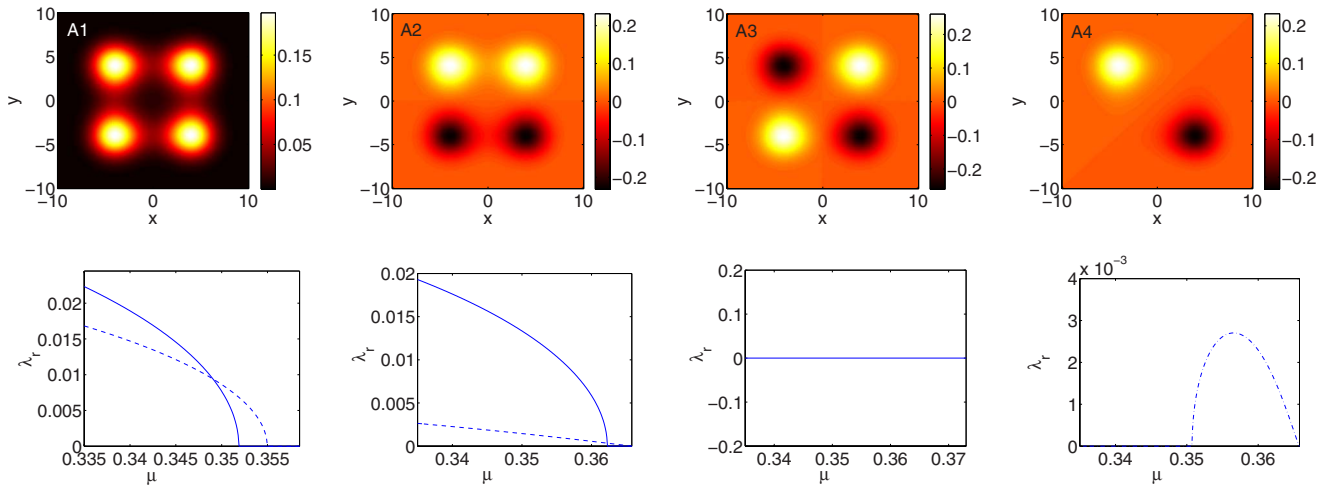


FIG. 4. (Color online) Top panels show the profiles of the wave functions corresponding to branches A1, A2, A3, and A4 (from left to right) at $\mu=0.34$. The bottom panels display real parts of the unstable eigenvalues for infinitesimal perturbations around the respective branches as functions of μ . The solid and dashed lines denote different pairs of real eigenvalues.

populated ones, branches B1-B3 feature two pairs of peaks with different amplitudes, branches C1-C4 have three different amplitudes, while D1 has all of its four peaks different. The waveforms in the top rows of Figs. 4–7 display prototypical realizations of the relevant branches, and their stability properties are illustrated, as a function of eigenvalue parameter μ , in the bottom rows.

We will now explain in detail solutions appearing in the full bifurcation diagram, starting from the linear limits ($N \rightarrow 0$). First, we look at the group of solutions related to branch A1, as shown in the bottom left panel of Fig. 3. This branch arises from the symmetric linear mode at $\mu = \omega_0$, i.e., the ground state in the linear limit, u_0 . Accordingly, A1 features four identically populated wells. The analysis demonstrates that it is stable near the linear limit, but soon gets destabilized, due to the emergence of branches C1 and B1, through subcritical and supercritical pitchfork bifurcations, respectively, around $\mu=0.355$. In other words, there are two consecutive *steady-state bifurcations*, in the language of Ref.

[31], in two different subspaces, in which one unstable solution, C1, collides with A1 and, simultaneously, a pair of eigenvalues emerges (in a subcritical pitchfork) on the real axis for branch A1 with the decrease of μ ; then, a supercritical pitchfork takes place in another subspace, in which B1 retains only one real pair, while another pair passes through the origin along branch A1. The actual “pitchfork” cannot be visualized here in the usual manner, because any of the four equivalent versions of B1 (obtained by the rotation through $\pi/2$) have the same value of N , being thus represented by the same curve in the graph. Branch B1, which is unstable due to a pair of real eigenvalues throughout its existence domain, features two of the wells on one side being less populated than the other two. Configuration B1 becomes increasingly more asymmetric as it deviates from A1. A noteworthy feature is shown by branch C1, which bifurcates from A1 at almost the same place as B1: after having emerged, it tends to be located on the left of A1, as are all other branches bifurcating from A1. However, within a narrow interval of μ ,

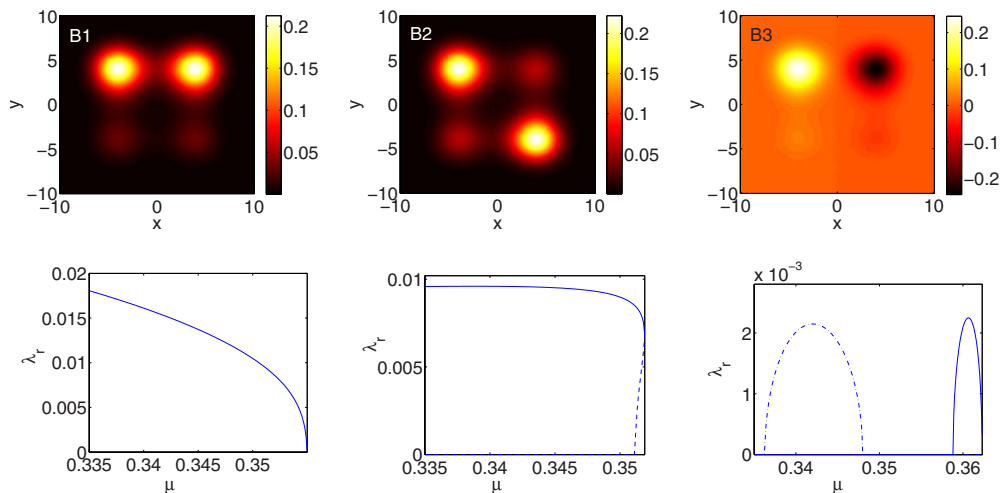


FIG. 5. (Color online) Top: profiles of the wave functions that correspond to branches B1, B2, and B3 (from left to right) at $\mu=0.34$. Bottom: real parts of unstable eigenvalues, associated with the respective branches, as a function of μ .

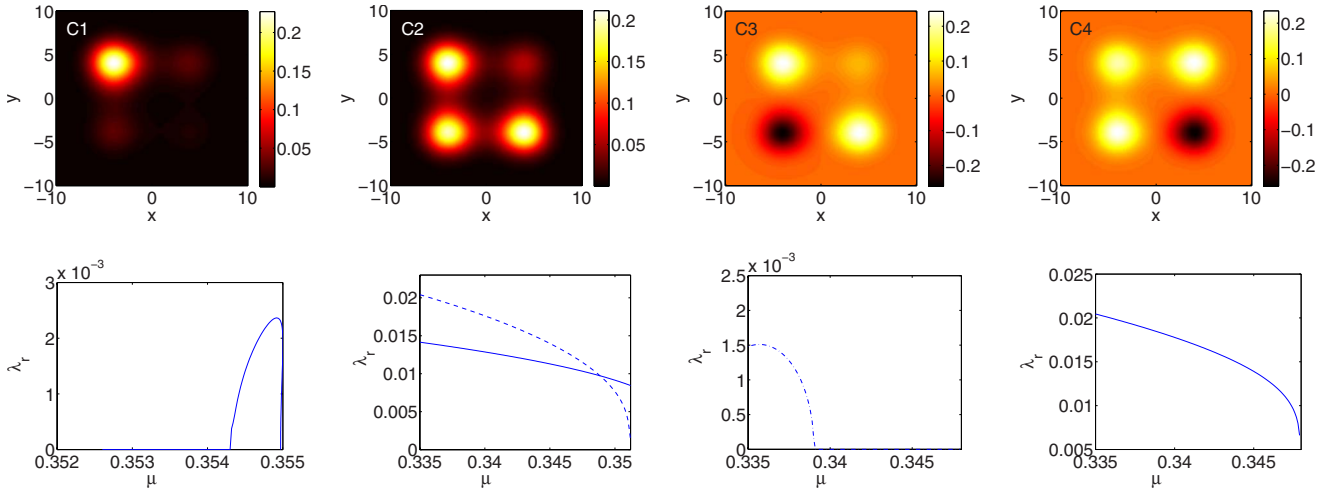


FIG. 6. (Color online) Top: profiles of the wave functions for branches C1, C2, C3, and C4 (from left to right) at $\mu=0.34$. Bottom: real parts of unstable eigenvalues, associated with the corresponding branches, versus μ .

its norm decreases ($dN/d\mu > 0$) slightly before starting to grow as usual ($dN/d\mu < 0$). Naturally, when the norm decreases the solution is destabilized and then it remains stable after the turning point, pursuant to the Vakhitov-Kolokolov criterion [32]. Branch A1 is endowed with two identical pairs of real eigenvalues by B1 and C1 upon their bifurcation (which is shown as the dashed line in the bottom left panel of Fig. 4). When another different pair of real eigenvalues occurs, it will be marked by a solid line. The dashed-dotted lines denote the complex quartets of eigenvalues. This notation holds in Figs. 4–7. As N grows further, a subsequent bifurcation, at $\mu=0.3519$, leading to the emergence of branch B2, adds yet another real eigenvalue pair to A1; this means that A1 possesses, in total, three real eigenvalue pairs for sufficiently large values of N . Branch B2 features two wells on the diagonal which are less populated than the other two, and it is unstable, through two pairs of real eigenvalues, near the point where it is created by the bifurcation from A1; however, one of the pairs is eliminated by the emergence of a new branch, C2, from B2 through a pitchfork shortly afterwards. Branch B2 then remains unstable with one real pair, while C2 (with three principal sites, one of which is of lesser amplitude than the other two) is unstable due to two real eigenvalue pairs.

The above description encompasses all branches of stationary solutions which can be traced back to the ground state of the linear system. Detailed information for the cor-

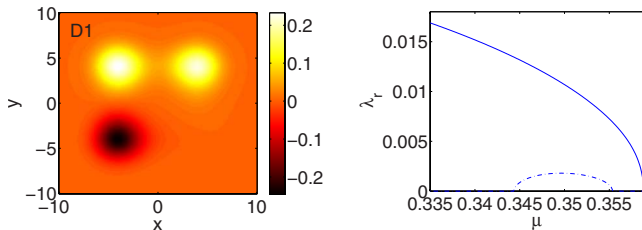


FIG. 7. (Color online) Left: the profile of the wave function of branch D1 at $\mu=0.34$. Right: real parts of its unstable eigenvalues versus μ . Notice the presence of a quartet, indicated by a dash-dotted line.

responding profiles of the wave function, and the development of the real eigenvalues associated to them, is presented in Figs. 4–6.

Next we turn to the states originating from the second linear mode, as shown in the bottom right panel of Fig. 3. Branch A2 starts from the respective eigenvalue, $\mu=\omega_1=\omega_2$, which pertains to the first and second (degenerate in the linear limit) excited states. This branch emerges as an unstable one, carrying a real eigenvalue pair. The respective wave-function profile features four wells populated with the same absolute values of the amplitude, but opposite signs on the two sides, see Fig. 4. Branch B3 emerges from A2 through a supercritical pitchfork at $\mu=0.3623$, lending another real eigenvalue pair to A2. Similar to the case of B1 (as it separates from A1), in state B3 two wells on one side tend to be less populated than the other two, as this branch moves farther from A2. Branch B3 remains unstable through one real eigenvalue pair, until getting stabilized by another pitchfork bifurcation, that takes place at $\mu=0.3589$; this bifurcation simultaneously gives rise to a new unstable branch, D1, that features different populations in all four wells. Notice that both B3 and D1 pass through a Hamiltonian-Hopf bifurcation (alias the 1:1 resonance, in terms of Ref. [31]), which means that, in the relevant parametric interval ($0.3362 < \mu < 0.348$ for B3, and $0.3444 < \mu < 0.3553$ for D1), B3 is destabilized by a complex quartet of small eigenvalues, while D1 remains unstable, but through one real eigenvalue pair and a complex quartet (the dash-dotted lines in the bottom right panels of Figs. 5 and 7 refer to this effect, i.e., the presence of a quartet).

Branch A4 bifurcates from the same linear mode as A2. It is unstable near the linear limit due to a Hamiltonian-Hopf bifurcation, but with the increase of N it becomes stable. Branch A4 features a waveform in which only two wells lying on the diagonal are populated, with the same amplitude but opposite signs.

Branch A3 arises from the third excited linear mode at $\mu=\omega_3$. In this case, two wells on the diagonal are populated with equal amplitudes, while in the other two the amplitudes are of opposite signs. It is the unique stationary solution

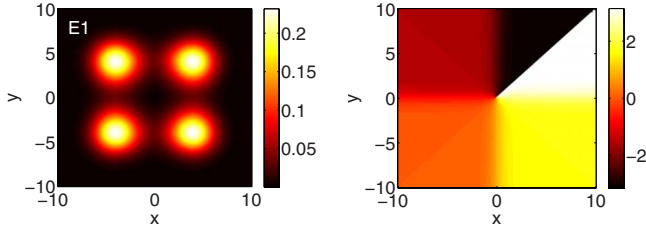


FIG. 8. (Color online) The absolute value (left) and phase (right) of a vortex state for $\mu=0.34$.

which remains *stable* across the *entire* bifurcation diagram (despite the fact that it has three pairs of purely imaginary eigenvalues with a negative Krein signature [33], which in principle, can give rise to Hamiltonian-Hopf bifurcations).

Finally, branches C3 and C4, which are located slightly below A2 in Fig. 3, correspond to a pair of states which arise through a saddle-node bifurcation at some critical value of the chemical potential ($\mu \approx 0.348$, for parameters of the model chosen in the present case). Branch C4 (the one with higher values of N) is unstable through a real eigenvalue pair, while C3 remains stable, except inside a short instability interval, which is accounted for by a Hamiltonian-Hopf bifurcation.

In addition to the above real stationary states, we have also found complex solutions in the form of vortices [21,30]. A typical example of such a solution is shown in Fig. 8. Throughout the regime of parameters considered herein, such solutions have been found to be *linearly stable*.

It is interesting to note that, for all the solutions considered herein, in the large- N limit, taking into account the criterion $N < N_{cr}$ so as to prevent the onset of the collapse, their stability characteristics coincide with what can be suggested by the discrete nonlinear Schrödinger (DNLS) model considered in Ref. [29] (see also Refs [34,35] for the corresponding 1D and 3D stability results). This is natural since effectively the four-mode reduction provides a four site, analog of the DNLS model with coupling γ_1 and on-site nonlinearity coefficient A_n . Since the analysis of [29] is based on a few-site reduction of the full (infinite lattice) model close to the anticontinuum limit (i.e., a strongly nonlinear limit), we expect that in the large- N limit the stability properties should be as expected from the full model. For the small- N (small nonlinearity) limit, the generalization is not immediate since the crosstalk among lattice sites plays a significant role and the finite size of the four-well setting may bear differences from the situation where more neighbors are involved. Gross features of the large- N limit are that, whenever two adjacent sites are in-phase, a real eigenvalue pair is expected to emerge due to their interaction, while whenever such sites are out-of-phase, the relevant eigenvalue is expected to be imaginary [36], but with a negative Krein signature [29], which, as mentioned above, implies a potential for a Hamiltonian-Hopf bifurcation. It should also be noted that, in the limit of the infinitely extended lattice, it is naturally expected that the asymmetries observed herein in many of the branches will disappear (i.e., the amplitudes in different wells will be equal)—see also a relevant discussion in Ref. [37].

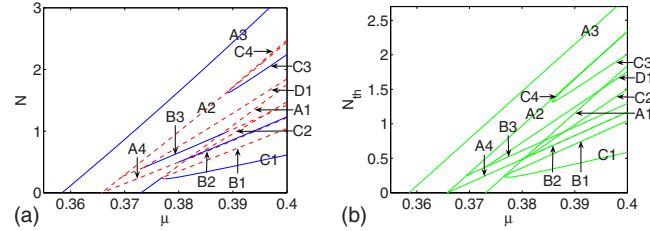


FIG. 9. (Color online) The norm of the numerical (left) and approximate (right) stationary solutions to Eq. (1) with the self-defocusing nonlinearity ($s=+1$), as a function μ (the chemical potential in BECs or propagation constant in optics). The labels of the branches are explained in the text.

B. Repulsive interactions

We now briefly discuss the case of the self-defocusing nonlinearity, which corresponds to $s=+1$ in Eq. (1), with the objective to highlight its similarities with and differences from the case of the attractive interactions. The bifurcation diagram for the model is displayed in Fig. 9.

The solutions are labeled so as to match the self-focusing case, by means of the appropriate *staggering transformation* [38]. The latter effectively converts the defocusing nonlinearity into a focusing one by changing the relative phase of nearest-neighbors from 0 to π and vice versa, while preserving the relative phase of next-nearest neighbors. In this way, each solution in the self-defocusing case is linked to its counterpart in the self-focusing model through this transformation. Following this relation, and adopting the same matrix symbolic representation as used for the focusing case in Sec. III A, the branches of solutions are labeled as follows: $A1 \equiv \begin{pmatrix} -1 & 1 \\ 1 & -1 \end{pmatrix}$, $A2 \equiv \begin{pmatrix} -1 & 1 \\ -1 & 1 \end{pmatrix}$, $A3 \equiv \begin{pmatrix} 1 & 1 \\ 1 & 1 \end{pmatrix}$, $A4 \equiv \begin{pmatrix} -1 & 0 \\ 0 & 1 \end{pmatrix}$, $B1 \equiv \begin{pmatrix} -1 & 1 \\ \varepsilon & -\varepsilon \end{pmatrix}$, $B2 \equiv \begin{pmatrix} -1 & \varepsilon \\ \varepsilon & -1 \end{pmatrix}$, $B3 \equiv \begin{pmatrix} -1 & -1 \\ \varepsilon & \varepsilon \end{pmatrix}$, $C1 \equiv \begin{pmatrix} -1 & \varepsilon \\ \varepsilon & -\varepsilon \end{pmatrix}$, $C2 \equiv \begin{pmatrix} -1 & \varepsilon \\ 1-\varepsilon & -1 \end{pmatrix}$, $C3 \equiv \begin{pmatrix} -1 & \varepsilon \\ -1-\varepsilon & -1 \end{pmatrix}$, $C4 \equiv \begin{pmatrix} -1 & \varepsilon \\ 1+\varepsilon & -1 \end{pmatrix}$, and $D1 \equiv \begin{pmatrix} -1 & 1-\varepsilon \\ -1-\varepsilon & \varepsilon \end{pmatrix}$.

Thus, in this case, the symmetric ground state of the system is A3, which is stable for arbitrary values of N . Branch A2 is immediately unstable, starting from the linear limit. B3 bifurcates from A2 and remains unstable before getting stabilized through giving birth to D1 (and then becoming destabilized again). Branch A1 is stable near the linear limit, but is subsequently destabilized due to bifurcations that give rise to B1 and C1, and an additional real eigenvalue pair arises at a higher value of N due to the emergence of B2, from which another new branch, namely, C2, arises in turn. Branches C3 and C4 exist for a while (when N is large enough), and then collide at $\mu=0.389$ (for the values of parameters adopted herein). The types of the bifurcations, the emergence of the corresponding solutions, and the corresponding stability properties were found to be in direct correspondence to the case of the self-focusing nonlinearity, provided that one takes into account the staggering transformation relating the self-repulsive and attractive models as indicated above.

C. Dynamics

We now proceed to investigate the time evolution of unstable states in the model with the self-focusing nonlinearity. To this end, for each unstable branch, a small perturbation is added as suggested by the most unstable eigenmode of the

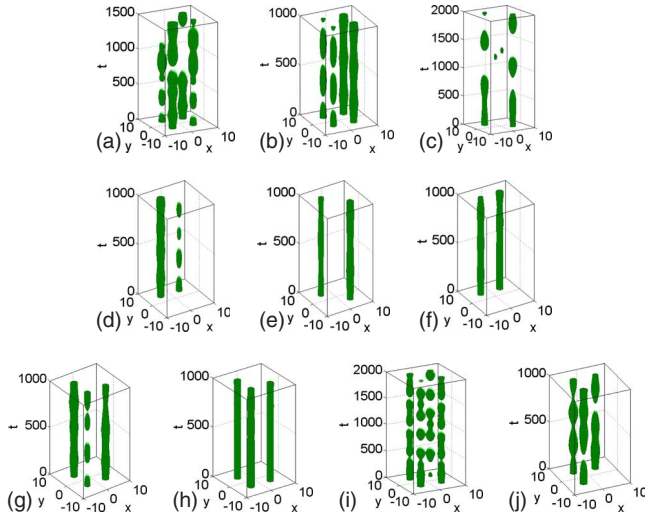


FIG. 10. (Color online) The spatiotemporal evolution of unstable states, represented by the respective density isosurface, $|u(x, y, t)|^2 = k$, where constant k is taken as half the maximum value of the density distribution at $t=0$. The results are arranged as follows. Top panels: A1, A2, A4; middle panels: B1, B2, B3; bottom panels: C2, C3, C4, D1.

linearization near the original stationary solution, at $\mu = 0.335$. We have adopted a fourth-order Runge-Kutta method in order to monitor the dynamical evolution of the system with a time step $\Delta t = 0.001$. Results of the simulations are presented in Fig. 10.

Panel (a) shows the behavior of solution A1, which, as a result of the instability, starts oscillating between a state where all four wells are populated and one in which only two diagonal wells are not empty. Panel (b) depicts a periodic oscillatory behavior of A2, also between four and two populated sites, but in this case the continuously populated sites are adjacent to each other. Unstable mode A4 (panel (c)) features only two nonempty wells, with the symmetry-breaking instability resulting in the oscillating enhanced population of one of the two. As explained in Sec. III A, modes B1, B2, and B3 have two very weakly populated wells, in comparison with the other two. Since the dynamics is plotted in Fig. 10 by means of isosurface $|u(x, y, t)|^2 = k$, where k is half the maximum density at $t=0$, the evolution in the weakly populated wells is not visible (which indicates that they play a minor role in the dynamics). Panel (d) shows that mode B1 features SSB similar to that of A4, but between adjacent sites. On the other hand, modes B2 and B3 appear to be mildly oscillating between the two dominant wells roughly periodically, as shown in panels (e) and (f). Mode C2 [in panel (g)] oscillates between three and two populated sites (the seemingly empty well is actually a weakly populated one, similarly to the modes of type B, see above). Mode C3, whose weak instability is caused by a quartet of eigenvalues, is also “breathing” within the respective set of three predominantly populated wells, as shown in panel (h). Finally, mode C4 [shown in panel (i)] involves a complex symmetry-breaking pattern, with different numbers of wells populated at different times, while mode D1 [panel (j)] oscillates between three- and two-well asymmetric configurations.

IV. CONCLUSION

In this work, we have studied stationary and dynamical properties of the two-dimensional nonlinear Schrödinger/Gross-Pitaevskii equation, which includes the four-well linear potential, with both signs of the nonlinearity, attractive and repulsive. The model applies to a pancake-shaped (planar) BEC, where the four-well potential can be generated by a combination of the harmonic trap and optical lattice (OL). The same model describes the propagation of an optical beam in a bulk nonlinear medium with an embedded four-channel guiding structure.

Our semianalytical approach was based on the four-mode truncation, which strongly simplifies the identification of stationary solutions. Using this approximation, we were able to find, first, four symmetric, and antisymmetric linear modes (two of which are identical), and then all branches of asymmetric solutions emerging from them, through the SSB (spontaneous-symmetry-breaking) mechanism, in the model with the self-focusing nonlinearity. The linear-stability analysis demonstrated how pitchfork and saddle-node bifurcations change the stability of the solution branches. We have also shown that, in the limit of the strong nonlinearity, properties of localized modes in the model with either sign of the nonlinearity can be understood on the basis of earlier known results pertaining to the corresponding discrete NLS model. In fact, the identification of the SSB modes specific to the four-well configuration in the 2D geometry presents new physical results obtained in this work. We have also described the evolution of all unstable solutions, directly observing the emergence of symmetry-breaking instabilities and the emergence of respective oscillating solutions.

It would be interesting to investigate how these four-site configurations may be embedded into a larger potential pattern, with 9 or 16 wells, and examine whether the SSB modes, considered in this work, are sustained (or how they are modified) within the larger pattern. In this context, a conjecture that calls for a proof is that, in the infinite periodic lattice formed by potential wells, the nonlinearity can support 2D solitons and localized vortices with various symmetries, but not confined asymmetric states. This conjecture is suggested by results reported for infinite linear [22–24,39] and nonlinear [40] potential lattices. Eventually, it may be relevant to extend the analysis of the SSB to the 3D space, the most natural respective setting being that based on a set of eight potential wells. The corresponding version of the NLS equation is not relevant in the context of nonlinear optics, but it remains a meaningful (and actually challenging) model for the BEC physics.

ACKNOWLEDGMENTS

P.G.K. gratefully acknowledges support from NSF-DMS-0349023 and NSF-DMS-0806762, as well as from the Alexander von Humboldt Foundation. The work of D.J.F. was partially supported by the Special Research Account of the University of Athens. B.A.M. acknowledges a partial support from the German-Israel Foundation through Grant No. 149/2006.

- [1] L. P. Pitaevskii and S. Stringari, *Bose-Einstein Condensation* (Oxford University Press, Oxford, 2003).
- [2] C. J. Pethick and H. Smith, *Bose-Einstein Condensation in Dilute Gases* (Cambridge University Press, Cambridge, 2002).
- [3] Yu. S. Kivshar and G. P. Agrawal, *Optical Solitons: From Fibers to Photonic Crystals* (Academic Press, San Diego, 2003).
- [4] *Emergent Nonlinear Phenomena in Bose-Einstein Condensates. Theory and Experiment*, edited by P. G. Kevrekidis, D. J. Frantzeskakis, and R. Carretero-González (Springer-Verlag, Berlin, 2008).
- [5] C. Sulem and P. L. Sulem, *The Nonlinear Schrödinger Equation* (Springer-Verlag, New York, 1999).
- [6] M. Albiez, R. Gati, J. Fölling, S. Hunsmann, M. Cristiani, and M. K. Oberthaler, Phys. Rev. Lett. **95**, 010402 (2005).
- [7] A. Weller, J. P. Ronzheimer, C. Gross, J. Esteve, M. K. Oberthaler, D. J. Frantzeskakis, G. Theocharis, and P. G. Kevrekidis, Phys. Rev. Lett. **101**, 130401 (2008).
- [8] I. Shomroni, E. Lahoud, S. Levy, and J. Steinhauer, Nat. Phys. **5**, 193 (2009).
- [9] S. Raghavan, A. Smerzi, S. Fantoni, and S. R. Shenoy, Phys. Rev. A **59**, 620 (1999); S. Raghavan, A. Smerzi, and V. M. Kenkre, *ibid.* **60**, R1787 (1999); A. Smerzi and S. Raghavan, *ibid.* **61**, 063601 (2000).
- [10] E. A. Ostrovskaya, Yu. S. Kivshar, M. Lisak, B. Hall, F. Cattani, and D. Anderson, Phys. Rev. A **61**, 031601(R) (2000).
- [11] K. W. Mahmud, J. N. Kutz, and W. P. Reinhardt, Phys. Rev. A **66**, 063607 (2002).
- [12] V. S. Shchesnovich, B. A. Malomed, and R. A. Kraenkel, Physica D **188**, 213 (2004).
- [13] D. Ananikian and T. Bergeman, Phys. Rev. A **73**, 013604 (2006).
- [14] P. Ziñ, E. Infeld, M. Matuszewski, G. Rowlands, and M. Trippenbach, Phys. Rev. A **73**, 022105 (2006).
- [15] T. Kapitula and P. G. Kevrekidis, Nonlinearity **18**, 2491 (2005).
- [16] G. Theocharis, P. G. Kevrekidis, D. J. Frantzeskakis, and P. Schmelcher, Phys. Rev. E **74**, 056608 (2006).
- [17] D. R. Dounas-Frazer, A. M. Hermundstad, and L. D. Carr, Phys. Rev. Lett. **99**, 200402 (2007).
- [18] T. Mayteevarunyoo, B. A. Malomed, and G. Dong, Phys. Rev. A **78**, 053601 (2008).
- [19] C. Cambournac, T. Sylvestre, H. Maillotte, B. Vanderlinden, P. Kockaert, Ph. Emplit, and M. Haelterman, Phys. Rev. Lett. **89**, 083901 (2002).
- [20] P. G. Kevrekidis, Z. Chen, B. A. Malomed, D. J. Frantzeskakis, and M. I. Weinstein, Phys. Lett. A **340**, 275 (2005).
- [21] K. J. H. Law, L. Qiao, P. G. Kevrekidis, and I. G. Kevrekidis, Phys. Rev. A **77**, 053612 (2008); K. J. H. Law, P. G. Kevrekidis, B. P. Anderson, R. Carretero-González, and D. J. Frantzeskakis, J. Phys. B **41**, 195303 (2008).
- [22] A. Gubeskys and B. A. Malomed, Phys. Rev. A **76**, 043623 (2007).
- [23] L. Gubeskys and B. A. Malomed, Phys. Rev. A **79**, 045801 (2009).
- [24] T. Mayteevarunyoo, B. A. Malomed, J. Opt. A, Pure Appl. Opt. **11**, 094015 (2009).
- [25] G. L. Alfimov, P. G. Kevrekidis, V. V. Konotop, and M. Salerno, Phys. Rev. E **66**, 046608 (2002).
- [26] L. Salasnich and B. A. Malomed, Phys. Rev. A **79**, 053620 (2009).
- [27] J. R. Marciante and G. P. Agrawal, IEEE J. Quantum Electron. **32**, 590 (1996); M. Brambilla, L. A. Lugiato, F. Prati, L. Spinelli, and W. J. Firth, Phys. Rev. Lett. **79**, 2042 (1997).
- [28] L. Bergé, Phys. Rep. **303**, 259 (1998).
- [29] D. E. Pelinovsky, P. G. Kevrekidis, and D. J. Frantzeskakis, Physica D **212**, 20 (2005).
- [30] T. Kapitula, P. G. Kevrekidis, and D. J. Frantzeskakis, Chaos **18**, 023101 (2008).
- [31] M. Dellnitz, I. Melbourne, and J. E. Marsden, Nonlinearity **5**, 979 (1992).
- [32] N. G. Vakhitov and A. A. Kolokolov, Radiophys. Quantum Electron. **16**, 783 (1973).
- [33] T. Kapitula, P. G. Kevrekidis, and B. Sandstede, Physica D **195**, 263 (2004).
- [34] D. E. Pelinovsky, P. G. Kevrekidis, and D. J. Frantzeskakis, Physica D **212**, 1 (2005).
- [35] M. Lukas, D. E. Pelinovsky, and P. G. Kevrekidis, Physica D **237**, 339 (2008).
- [36] T. Kapitula, P. G. Kevrekidis, and B. A. Malomed, Phys. Rev. E **63**, 036604 (2001).
- [37] T. Kapitula, P. G. Kevrekidis, and Z. Chen, SIAM J. Appl. Dyn. Syst. **5**, 598 (2006).
- [38] P. G. Kevrekidis, H. Susanto, and Z. Chen, Phys. Rev. E **74**, 066606 (2006).
- [39] R. Driben, B. A. Malomed, A. Gubeskys, and J. Zyss, Phys. Rev. E **76**, 066604 (2007); R. Driben and B. A. Malomed, Eur. Phys. J. D **50**, 317 (2008).
- [40] Y. V. Kartashov, B. A. Malomed, V. A. Vysloukh, and L. Torner, Opt. Lett. **34**, 770 (2009); F. W. Ye, Y. V. Kartashov, B. Hu, and L. Torner, Opt. Express **17**, 11328 (2009).